CHEMISTRY OF MATERIALS
Article

Chem. Mater. **2010,** *22,* 3251–3258 3251
DOI:10.1021/cm100491r

Chemistry of Trimethyl Aluminum: A Spontaneous Route to Thermally Stable 3D Crystalline Macroporous Alumina Foams with a Hierarchy of Pore Sizes

Yu Li,[†,‡,⊥] Xiao-Yu Yang,[†,‡,⊥] Ge Tian,[‡] Aurélien Vantomme,[‡,#] Jiaguo Yu,[†] Gustaaf Van Tendeloo,[§] and Bao-Lian Su*[,†,‡]

[†]*State Key Laboratory of Advanced Technology for Materials Synthesis and Processing, Wuhan University of Technology, 122 Luoshi Road, 430070, Wuhan, Hubei, People's Republic of China,* [‡]*Laboratory of Inorganic Materials Chemistry (CMI), University of Namur (FUNDP), 61, rue de Bruxelles, B-5000 Namur, Belgium,* [§]*EMAT, University of Antwerp, Groenenborgerlaan 171, B-2020 Antwerpen, Belgium, and* [#]*Present address: Total Petrochemicals Research Feluy, Polyolefins Catalysis Department, Zoning 1C, B-7181 Feluy, Belgium.* [⊥]*These two authors equally contributed to this paper.*

Received February 17, 2010. Revised Manuscript Received April 15, 2010

A simple and spontaneous one-pot self-formation procedure that is easy to scale up has been developed based on the chemistry of trimethylaluminum (TMA), leading to thermally stable macroporous crystalline alumina with a very unique and unprecedented three-dimensional (3D) hierarchical pore structure consisting of well-defined wormlike mesopores. TMA is the precursor of both product and porogene (viz, two working functions within the same molecule (2 in 1)). The materials obtained have been intensively characterized by powder X-ray diffraction (XRD), field-emission scanning electron microscopy (FESEM), high-resolution transmission electron microscopy (HRTEM), N_2 adsorption−desorption, and mercury porosimetry. The open cagelike macrocavities are self-constructed by mesoporous nanorods (diameter of ca. 40−70 nm), which are themselves formed by a random assembly of fibrous nanoparticles 5−6 nm in size. Optical microscopy (OM) has been used in situ to follow the synthesis procedure, which led to the proposal of the formation mechanism. Methane molecules as porogens, which were instantaneously released because of the fast hydrolysis of the chemical precursor, were the key factor in producing these 3D structures with uniform co-continuous macropores that interconnected directly with the wormlike mesopores. The important characteristic of this procedure is the concurrent formation of a multiscaled porous network. The material exhibits great thermal stability. The hierarchically mesoporous−macroporous Al_2O_3 obtained is quite attractive for a myriad of applications, from catalysis to biomedicine. The present work illustrates that the one-pot self-formation concept, based on the chemistry of alkyl metals, is a versatile method to design industrially valuable hierarchically porous materials.

1. Introduction

Materials with a hierarchically interconnected pore system on micro−meso−macro length scales have recently attracted considerable attention, because of their potential technological and biomedical applications as catalysts, adsorbents, bone tissue regeneration matrices, and scaffolds to grow cardiac tissue, as well as for the entrapment of bacteria and plant cells to exploit the photosynthesis.[1−12]

Fluidizing catalytic cracking (FCC) catalysts are concrete examples of hierarchical structures currently in use in industry. They are composites formed by artificially mixing the main component (typically a USY zeolite that possesses mesoporosity generated via a steam dealumination treatment) with a macroporous matrix (usually amorphous silica, alumina, or silica/alumina with clay).[13−15] Many successful procedures have been invented to prepare

*Author to whom correspondence should be addressed. Tel.: +32 81 724531, + 86 27 87 66 52 57. Fax: +32 81 72 54 14. E-mails: baoliansu@whut.edu.cn, bao-lian.su@fundp.ac.be.

(1) Engelmayr, G. C.; Cheng, M. Y.; Bettinger, C. J.; Borenstein, J. T.; Langer, R.; Freed, L. E. *Nature Mat.* **2008**, *7*, 1003.
(2) Maekawa, H.; Esquena, J.; Bishop, S.; Solans, C.; Chmelka, B. F. *Adv. Mater.* **2003**, *15*, 591.
(3) Marolt, D.; Augst, A.; Freed, L. E.; Vepari, C.; Fajardo, R.; Patel, N.; Gray, M.; Farley, M.; Kaplan, D.; Vunjak-Novakovic, G. *Biomaterials* **2006**, *27*, 6138.
(4) Backov, R. *Soft Matter* **2006**, *2*, 452.
(5) Antonietti, M.; Berton, B.; Goltner, C.; Hentze, H. P. *Adv. Mater.* **1998**, *10*, 154.
(6) Yang, P.; Deng, T.; Zhao, D.; Feng, P.; Pine, D.; Chmelka, B. F.; Whitesides, G. M.; Stucky, G. D. *Science* **1998**, *282*, 2244.
(7) Holland, B. T.; Abrams, L.; Stein, A. *J. Am. Chem. Soc.* **1999**, *121*, 4308.
(8) Lebeau, B.; Fowler, C. E.; Mann, S.; Farcet, C.; Charleux, B.; Sanchez, C. *J. Mater. Chem.* **2000**, *10*, 2105.
(9) Rooke, J. C.; Léonard, A.; Su, B. L. *J. Mater. Chem.* **2008**, *18*, 1333.
(10) Rooke, J. C.; Léonard, A.; Sarmento, H.; Descy, J. P.; Su, B. L. *J. Mater. Chem.* **2008**, *18*, 2833.
(11) Meunier, Ch. F.; Van Cutsem, P.; Kwon, Y. U.; Su, B. L. *J. Mater. Chem.* **2009**, *19*, 1535.
(12) Meunier, Ch. F.; Van Cutsem, P.; Kwon, Y. U.; Su, B. L. *J. Mater. Chem.* **2009**, *19*, 4131.
(13) Léonard, A.; Su, B. L. *Chem. Commun.* **2004**, 1674.
(14) Leonard, A.; Su, B. L. *Colloids. Surf. A* **2007**, *300*, 129.
(15) Vantomme, A.; Leonard, A.; Yuan, Z. Y.; Su, B. L. *Colloids Surf., A* **2007**, *300*, 70.

Published on Web 04/27/2010

this type of material by dual exotemplating methods. Mesoporous−macroporous SiO_2 has been created by a combination of both surfactant and colloidal crystal templating techniques, using polymeric spheres and/or surfactant molecules.[5−8] An emulsion templating strategy in which uniformly dispersed oil droplets and surfactants has been smartly used. Antonelli reported a very elegant synthesis of macroporous−mesoporous niobium oxides by means of a NaCl-promoted vesicle templating method, using a niobium ethoxide/amine gel.[16] Other templates, such as gas bubbles,[2,17−19] supramolecular aggregates,[20−22] and biomaterials,[23−27] as well as other chemical and physical methods, such as the control of procedural conditions (synthesis and aging),[28] phase separation,[29−31] and post-treatment,[32,33] as well as the introduction of structural units with their own inherent porosity,[34−36] have been successfully employed. However, preparing porous inorganic materials without exotemplates, or at least without the intermediation of ordered arrays of surfactants, emulsions, and colloids, is still a very difficult task to reach.

It has been reported that hierarchically structured mesoporous−macroporous metal oxides with a variety of chemical compositions (aluminosilicates,[13−15,37] Al_2O_3,[14,15,37−39] ZrO_2,[14,15,20,37,40−44] TiO_2,[14,15,20,37,40−46] Y_2O_3,[14,15,20,37,40−42,46] Nb_2O_5,[14,15,20,37,40−42,46] and mixed oxides[14,15,20,37,40−42,46]), possessing well-ordered funnel-like macrochannels with mesoporous walls can be targeted without exotemplates via a "one-pot" self-formation process, based on the chemistry of metal alkoxides.[13−15,39,43−47] The key point of this novel synthesis process is the very high rate at which the hydrolyzed metal alkoxide species undergo condensation reactions in aqueous solution. When the metal alkoxide precursor comes into contact with water, hydrolysis begins. The reaction is instantaneous and causes alcohol molecules to be liberated with some force from the nucleation sites, generating within the product a porous network comprised of funnel-like macrochannels with hierarchically mesostructured porous walls. These alcohol molecules can thus be considered as the "porogene". Metal alkoxides play the role of the precursor of the final product and also the generator of porogene: two functions in one sole molecule (2 in 1). Shanks et al., Mann et al., and our group have recently reported very comprehensive and systematic works contributing toward a better understanding of the formation mechanism.[13−15,39,44−47] One of the important advantages of this preparation method, compared to other synthesis methods, is the direct production of pure oxide materials with hierarchical porosity. Another benefit is its simplicity, because no post-treatment, such as calcination or solvent extraction to remove any external templating agent, is necessary. Last, but not least, is the ease at which scaling up can be achieved to satisfy industrial requirements. This method can be easily combined with other strategies—for example, surfactant templating—to target even more-sophisticated porous structures ideal for catalytic nanoreactors.[48]

Instead of metal alkoxides, which can release alcohol molecules as self-generated "porogene molecules", one can imagine other precursors that can release "porogene molecules" in liquid and even gas form. Therefore, the great challenge is to find or to synthesize suitable chemical precursors.

Al_2O_3 is a major engineering material and offers a combination of good mechanical properties, corrosion resistance, low loss tangent, and controllable acido-basicity and electrical properties, leading to a wide range of applications and thus a major field of research. Porous Al_2O_3 is a very well-known catalyst support and drying agent; it is extensively used in a variety of catalytic reactions and separation processes.[49−51] Because of its chemical resistance and thermal stability, it is often used as a reference material in a variety of standardization and calibration procedures. Hierarchically tubelike mesoporous−macroporous

(16) Antonelli, D. M. *Microporous Mesoporous Mater*. **1999**, *33*, 209.
(17) Bagshaw, S. A. *Chem. Commun*. **1999**, 767.
(18) Carn, F.; Masse, P.; Sadaoui, H.; Julian, B.; Deleuze, H.; Ravaine, S.; Sanchez, C.; Talham, D. R.; Backov, R. *Langmuir* **2006**, *22*, 5469.
(19) Suzuki, K.; Ikari, K.; Imai, H. *J. Mater. Chem*. **2003**, *13*, 1812.
(20) Blin, J. L.; Léonard, A.; Yuan, Z. Y.; Gigot, L.; Vantomme, A.; Cheetham, A. K.; Su, B. L. *Angew. Chem., Int. Ed*. **2003**, *42*, 2872.
(21) Yuan, Z. Y.; Ren, T. Z.; Azioune, A.; Pireaux, J. J.; Su, B. L. *Chem. Mater*. **2006**, *18*, 1753.
(22) Chen, H.; Gu, J.; Shi, J.; Liu, Z.; Gao, J.; Ruan, M.; Yan, D. *Adv. Mater*. **2005**, *17*, 2010.
(23) Davis, S. A.; Burkett, S. L.; Mendelson, N. H.; Mann, S. *Nature* **1997**, *385*, 420.
(24) Cook, G.; Timms, P. L.; Goeltner-Spickermann, C. *Angew. Chem., Int. Ed*. **2003**, *42*, 557.
(25) Hall, S. R.; Bolger, H.; Mann, S. *Chem. Commun*. **2003**, 2784.
(26) Valtchev, V.; Smaihi, M.; Faust, A. C.; Vidal, L. *Chem. Mater*. **2003**, *16*, 1350.
(27) Yang, X.; Li, Z.; Liu, B.; Klein-Hofmann, A.; Tian, G.; Feng, Y.; Ding, Y.; Su, D.; Xiao, F. *Adv. Mater*. **2006**, *18*, 410.
(28) Hsu, Y. C.; Hsu, Y. T.; Hsu, H. Y.; Yang, C. M. *Chem. Mater*. **2007**, *19*, 1120.
(29) Nakanishi, K. *J. Porous Mater*. **1997**, *4*, 67.
(30) Konishi, J.; Fujita, K.; Nakanishi, K.; Hirao, K. *Chem. Mater*. **2006**, *18*, 6069.
(31) Huesing, N.; Raab, C.; Torma, V.; Roig, A.; Peterlik, H. *Chem. Mater*. **2003**, *15*, 2690.
(32) Yuan, Z. Y.; Blin, J. L.; Su, B. L. *Chem. Commun*. **2002**, 504.
(33) Panda, M.; Rajamathi, M.; Seshadri, R. *Chem. Mater*. **2002**, *14*, 4762.
(34) Caruso, R. A.; Schattka, J. H. *Adv. Mater*. **2000**, *12*, 1921.
(35) Caruso, R. A.; Antonietti, M. *Adv. Funct. Mater*. **2002**, *12*, 307.
(36) Giunta, P. R.; Washington, R. P.; Campbell, T. D.; Steinbock, O.; Stiegman, A. E. *Angew. Chem., Int. Ed*. **2004**, *43*, 1505.
(37) Vantomme, A.; Léonard, A.; Yuan, Z. Y.; Su, B. L. *Key Eng. Mater*. **2007**, *336*−*338*, 1933.
(38) Deng, W.; Toepke, M. W.; Shanks, B. H. *Adv. Funct. Mater*. **2003**, *13*, 61.
(39) Deng, W.; Shanks, B. H. *Chem. Mater*. **2005**, *17*, 3092.
(40) Vantomme, A.; Yuan, Z. Y.; Su, B. L. *New J. Chem*. **2004**, *28*, 1083.
(41) Yuan, Z. Y.; Vantomme, A.; Léonard, A.; Su, B. L. *Chem. Commun*. **2003**, 1558.
(42) Su, B. L.; Léonard, A.; Yuan, Z. Y. *C. R. Chim*. **2005**, *8*, 713.
(43) Ren, T. Z.; Yuan, Z. Y.; Su, B. L. *Chem. Commun*. **2004**, 2730.
(44) Hakim, S. H.; Shanks, B. H. *Chem. Mater*. **2009**, *21*, 2027.
(45) Collins, A.; Carriazo, D.; Davis, S. A.; Mann, S. *Chem. Commun*. **2004**, 568.
(46) Yang, X. Y.; Li, Y.; Lemaire, A.; Yu, J. G.; Su, B. L. *Pure Appl. Chem*. **2009**, *81*, 2265.
(47) Su, B. L.; Vantomme, A.; Surahy, L.; Pirard, R.; Pirard, J. P. *Chem. Mater*. **2007**, *19*, 3325.
(48) Yang, X. Y.; Li, Y.; Van Tendeloo, G.; Xiao, F. S.; Su, B. L. *Adv. Mater*. **2009**, *21*, 1368.
(49) Maeda, K.; Mizukami, F.; Watanabe, M.; Arai, N.; Niwa, S.; Toba, M.; Shimizu, K. *J. Mater. Sci. Lett*. **1990**, *9*, 522.
(50) Garcin, E.; Cartier, Cl. B.; Quemere, E. U.S. Patent 5,288,849, **1994**.
(51) Frank, M. M.; Chabal, Y. J.; Wilk, G. D. *Appl. Phys. Lett*. **2003**, *82*, 4758.

Al_2O_3 has recently been reported by both our group[21] and Shanks et al.,[38] using aluminum alkoxide precursors.

Trimethylaluminum ($Al(CH_3)_3$, TMA) is an industrially important organoaluminum compound, which is widely used in semiconductor fabrication to grow high-k dielectric Al_2O_3 thin films via atomic layer deposition (ALD) under H_2O vapor conditions. It is well-known that methane molecules can be generated by a very fast and spontaneous reaction between TMA and hydroxyl groups:[51,52]

$$Al(CH_3)_3 + 2H_2O \rightarrow AlOOH + 3CH_4$$

The question then arises as to whether methane molecules, released during the aforementioned reaction, play the role of "porogene", cf. alcohol molecules liberated during the hydrolysis of metal alkoxides, which would lead to the formation of macropores. The hydrolysis reaction of TMA is an exothermic reaction. The heat produced will accelerate the expulsion of small methane molecules, which can diffuse easily throughout the forming product, potentially generating 3D macroporous structures.

Here, we present the successful preparation of alumina possessing a 3D hierarchical pore structure with uniform co-continuous cagelike macropores constructed from well-defined wormlike mesoporous nanorods, via methane (CH_4) as endoporogene molecules, released instantaneously during the hydrolysis of TMA. The nanorods are formed by the random aggregation of nanofibers. This was achieved based on the chemistry of TMA. TMA plays two roles simultaneously: it is both the precursor of the product and the porogene. Therefore, like metal alkoxides, it is deemed to have two functions in one molecule (2 in 1). Very pure Al_2O_3 materials can be prepared starting with just the TMA precursor in aqueous solution, as opposed to other synthesis strategies where the resultant Al_2O_3 materials are often contaminated by residual species. Another major advantage of this process is that gaseous methane released from the reaction can be easily recovered and stocked for further utilization. This new process, which renders possible the precise control of the structure on the molecular scale, could be of great interest and, therefore, is a significant advance toward the understanding of the formation mechanism of these hierarchically structured porous materials.

2. Experimental Section

2.1. Synthesis. A 2.0 M trimethylaluminum ($Al(CH_3)_3$, TMA) solution in toluene was the only chemical reagent, which was purchased from Aldrich and used as received. For a typical synthesis, a flat evaporating dish was first filled with water (50 mL), then the TMA solution (3 mL, 2.0 M) was dropped into the flat evaporating dish until a layer of foam fully covered the surface of the water. The flat evaporating dish then was moved into an oven and dried at 40 °C overnight. Finally, a white solid product was collected and ground to a fine powder for further thermal treatment and characterization.

In the thermal treatment process, the as-synthesized product was placed into a muffle oven and was calcined at a set temperature and predetermined duration, such as 500 °C for 2 h and 900 °C for 2 h and 900 °C for 48 h. Finally, the calcined products were collected and reground for further characterization.

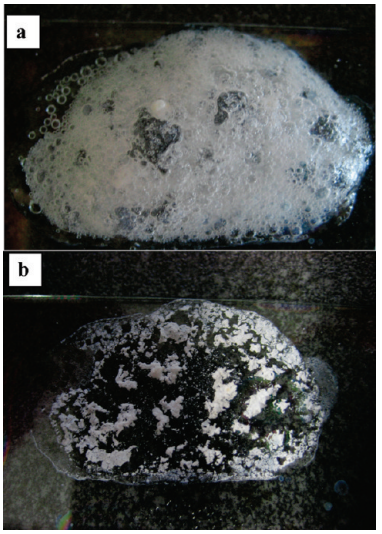

Figure 1. Ordinary photographs of (a) the product obtained directly after synthesis and (b) the dried product.

2.2. Characterization. X-ray diffraction (XRD) patterns were obtained with a Panalytical X'Pert diffractometer using Cu Kα radiation (λ = 1.54056 Å). Scanning electron microscopy (SEM) experiments were performed on a Model JSM-7500F electron microscope (JEOL, Japan). Transmission electron microscopy (TEM) experiments were performed on a Philips Model CM20 system with an acceleration voltage of 200 kV. High-resolution transmission electron microscopy (HRTEM) experiments were performed on a Model JEM-4000EX (JEOL, Japan) with an acceleration voltage of 400 kV. The nitrogen adsorption and desorption isotherms were measured at the temperature of liquid nitrogen using a Micromeritics Model ASAP 2010 M system. The pore size distribution curve (30−300 nm) obtained via mercury porosimetry was measured using a Micromeritics Model AutoPore IV 9500 system. All the samples were degassed for 12 h at 150 °C before analysis. The pore size distribution for mesopores was calculated using the Barrett−Joyner−Halenda (BJH) model.

3. Results and Discussion

3.1. 3D Crystalline Macroporous Foamlike Materials with Mesoporous Nanorods as Construction Scaffolds. To facilitate direct observation of material formation, the experiment was realized in a flat evaporating dish. A thin layer of water was deposited in this dish, to which a TMA droplet was added. Methane gas was instantaneously released as soon as the TMA droplet was in contact with water. This could be directly visualized. After only a few seconds, a continuous translucent gelatinous layer with significant porosity was formed. There was also the presence of a huge number of bubbles on the surface of the water. The entire synthesis procedure was followed in situ via optical microscopy. Figure 1a shows an ordinary photograph of the material obtained. The gelatinous translucent layer, containing a huge number of bubbles, is very swollen. The drying process yields a white powdery solid product (see Figure 1b). Figure 2 demonstrates typical SEM images and the proposed model of the macrostructure.

(52) Halls, M. D.; Raghavachari, K.; Frank, M. M.; Chabal, Y. *Phys. Rev. B* **2003**, *68*, 161302.

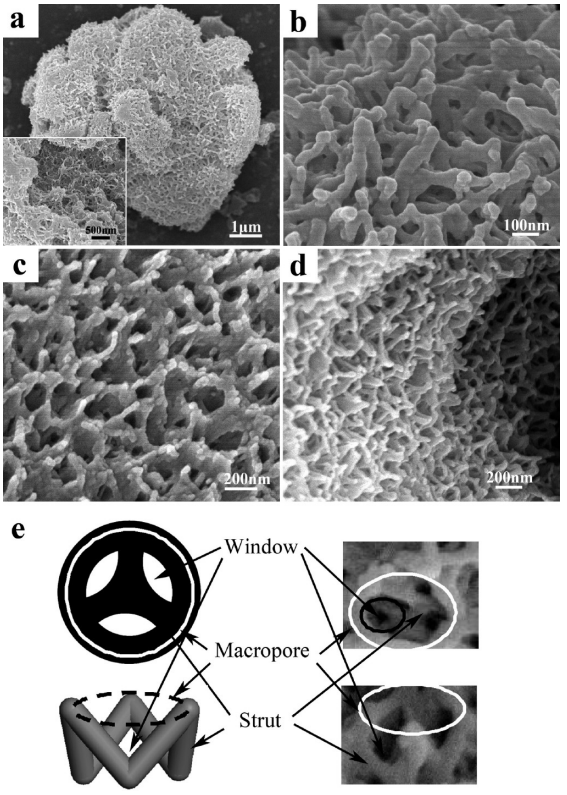

Figure 2. SEM images of the as-synthesized product: (a) low magnification of a large particle; (b) high magnification of the same particle in panel (a); (c) side view of the as-synthesized product; and (d) cross section of a crushed particle of the as-synthesized product. Panel (e) shows the proposed model of the macroporous structure; the upper and lower images of the right side were taken from panels (b) and (d), respectively.

Figure 2a depicts monolithic foamlike particles 10−30 μm in size. The materials have definable macropores, formed by the 3D net-cross structure. At higher magnification, it is confirmed that the macrocavities interconnect each other via a skeleton of nanorods ∼40−70 nm in diameter (Figure 2b). A side view of the macroporous system additionally shows that the external, open macropores have a regular diameter of ∼200 nm (see Figure 2c). The cross section of one large particle (Figure 2d) clearly indicates that the entire sample is a 3D structure constructed by the cross-linked nanorods. The external surface of the large particles is covered by a forest of homogeneous Λ-shaped nanorods. A simplified model of the macroporous structure (left side of Figure 2e) is proposed based on the above SEM observations (right side of Figure 2e), to aid the reader. The model illustrates the fine structure of the macropores formed by methane bubble templating.[13−15,39,43−48] The upper left side of the model is a plan view of a macrocavity and window, and the lower left side shows the simulated 3D macrocavity entrances that are constructed by the nanorods. Notably, the spontaneously generated structures consist precisely of a co-continuous skeleton surrounding the uniform distribution of open macropores (∼200 nm). The macrocavities are interconnected through windows (∼50−80 nm) that are probably formed as a result of contact between the methane bubbles that are released prior to formation of the AlOOH inorganic species. A phase-separation phenomenon (gas−solid) occurs.[29−31] We will discuss the formation mechanism further in the following section.

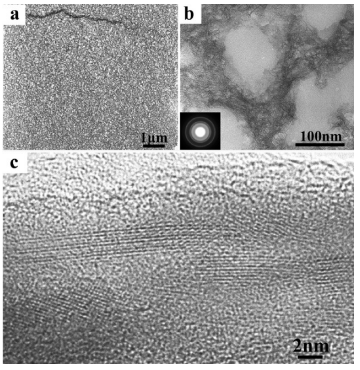

Figure 3. TEM images of the as-synthesized product: (a) low magnification of a microtomed large particle; (b) higher magnification of the same particle in panel (a), taken from different viewing angles; and (c) HRTEM image of the nanofiber-like structure. The inset in panel (b) is the corresponding selected area electron diffraction (SAED) pattern of the large particle in panel (a).

These 3D structures, constructed by the cross-linked nanorods, were characterized in further detail using TEM on ultramicrotomed specimens. Figure 3a presents a typical low-magnification image of one monolithic particle. The image of the microsection confirms that the 3D macroporous structure extends throughout the entire particle. Higher-magnification images of the cross-sectional material reveal more-detailed information of the foamlike macroporous structure (see Figure 3b). The image shows that the diameter of the nanorod-like structure, found between the macropores with quasicircular apertures, is ∼40−70 nm, which is consistent with the SEM observations and the proposed model that describes the macropore shape. The corresponding selected area electron diffraction (SAED) pattern (see the inset of Figure 3b) indicates that the as-synthesized product has a polycrystalline structure. Furthermore, Figure 3b illustrates that the nanorod-like walls of the macropores are constructed from a random aggregation of fibrous nanoparticles, which generates wormlike mesopores. The nanofibers, which are 5−6 nm in diameter, are clearly illustrated by HRTEM (see Figure 3c). An amorphous layer is found covering the crystalline nanofiber. The wormhole-like structure with its relatively homogeneous size of mesopores is further confirmed by the corresponding low-angle XRD pattern (see Figure 4a). Within this 2θ range, the pattern exhibits a single yet broad reflection, which indicates a disordered mesostructure. The reflection in the low-angle XRD pattern is an indication of the distance between nearest neighbors. The wide-angle XRD pattern (Figure 4b) exhibits diffraction lines that are assignable to the boehmite phase AlOOH (JCPDS File Card No. 21-1307). This kind of crystalline phase was often formed at room temperature as previously reported.[21] The weak and broad diffraction peaks indicate that the sample is composed of small crystals with a crystalline size on the nanometer scale, as previously verified by TEM observations.

The N_2 adsorption isotherms of the as-synthesized product (Figure 4c and Table 1) exhibit a type IV adsorption curve assigned to a mesostructure. The sharp increase

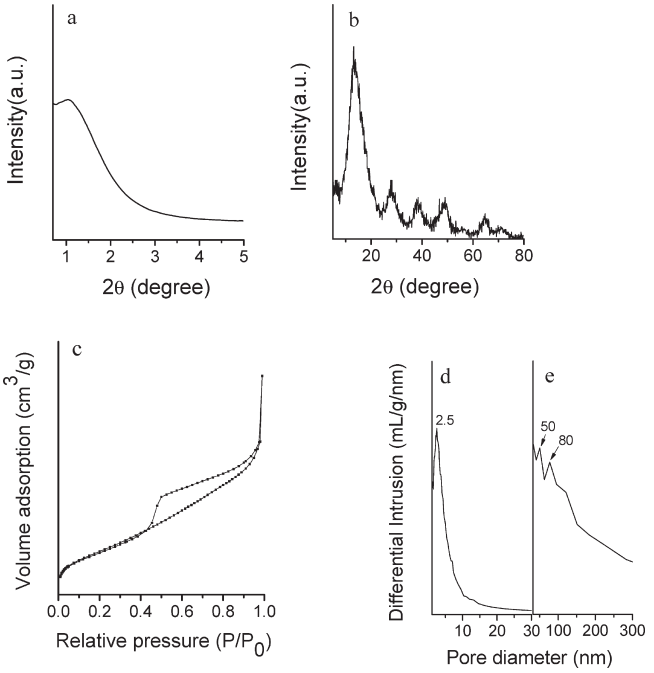

Figure 4. (a) Low-angle X-ray diffraction (XRD) patterns of the as-synthesized product; (b) wide-angle X-ray diffraction (XRD) patterns of the as-synthesized product; (c) N_2 adsorption−desorption isotherms; (d) corresponding pore size distribution curves of the as-synthesized product obtained by N_2 adsorption−desorption isotherms (0−30 nm) and mercury porosimetry measurements (30−300 nm).

Table 1. Textural Properties of the As-Synthesized AlOOH Product and the Products Calcined at Different Temperatures and Durations

sample	*d*-spacing (nm)	BET surface area (m^2/g)	pore volume (cm^3/g)	pore diameter (nm)
as-synthesized	8.5	425	0.60	2.5
500, 2 h	11.8	413	0.57	3.5
900, 2 h	11.8	179	0.56	7.4
900, 48 h	11.8	179	0.57	10.3

in N_2 adsorption volume at high p/p_0 values clearly indicates the presence of a significant degree of macroporosity. N_2 adsorption reveals a very high BET surface area of 425 m^2/g and a pore volume of 0.60 cm^3/g. The pore size distribution obtained from the Barrett−Joyner−Halenda (BJH) method applied to the adsorption branch of the isotherm gives a pore size of ∼2.5 nm (see Figure 4d). Notably, the larger pores centered at two different values, at ∼50 and 80 nm, are detected by mercury porosimetry measurements (see Figure 4e), which implies that the product contains an appreciable amount of large pores in the macropore range. It is highly probable that the 50- and 80-nm values correspond to two different macrocavity openings. These results are in good agreement with the SEM and TEM observations. Macroporous openings of 200 nm observed on the external surface of the monolithic particles are not revealed by mercury porosimetry. This is most probably due to the fact that these sizes correspond to the internal diameter of the cagelike macrocavities. Only the diameter of window entrances pore apertures can be accessed via mercury porosimetry.

The thermal stability of the 3D mesoporous−macroporous structures was studied by subjecting the as-synthesized

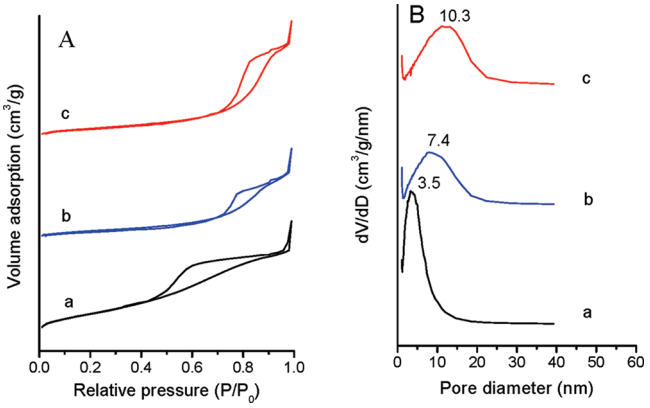

Figure 5. (A) N_2 adsorption−desorption isotherms and (B) the corresponding pore size distribution curves of the samples calcined at different temperatures and durations. (Legend: isotherm a, 500 °C for 2 h; isotherm b, 900 °C for 2 h; and isotherm c, 900 °C for 48 h. Isotherms b and c are displaced upward for clarity.)

product to thermal treatments at 500 and 900 °C. Figure 5 shows the N_2 isotherms (Figure 5A) and pore size distributions (Figure 5B) of various thermally treated products. Their textural characteristics are presented in Table 1. After calcination at 500 °C for 2 h, 900 °C for 2 h, and 900 °C for 48 h, the products clearly exhibit a typical type IV isotherm assigned to mesostructures (Figure 5A). Importantly, the isotherms of the calcined products still present two inflections, similar to the as-synthesized product (see Figure 4c). The first one corresponds to a mean pore size of ∼3.5−10.3 nm. The second inflection at high p/p_0 values indicates the presence of a significant amount of large pores. These results show that the macroporous alumina with hierarchical pores is extremely stable during exposure to high temperatures and long-term thermal treatment. After a 2 h treatment at 500 °C, the BET surface area and primary mesopore volume have scarcely changed from the values obtained on the as-synthesized product (Table 1). Even when the sample is subjected to a high-temperature treatment at 900 °C for 48 h, well-defined type IV isotherms (isotherm c in Figure 5A) are obtained. Although the pore size distribution becomes larger and is shifted from 3.5 nm to 10.3 nm (Figure 5B), the BET surface area is still high for a well-crystallized material[53,54] and the mesopore size distribution remains relatively narrow (Figure 5B). This is consistent with the well-resolved XRD pattern (Figure 6), confirming the remarkable thermal stability of the macroporous alumina with hierarchical pores.

All the calcined products displayed one peak in the low-angle range (Figure 6A) and there is almost no obvious peak shift when comparing to the as-synthesized product, indicating that the lattice parameters of the calcined products did not change and the mesostructure was preserved after calcination. The wide-angle diffractograms of the calcined products further indicate an increase in the extent of crystallinity. After calcination at 500 °C (pattern a in

(53) Yang, X.; Han, Y.; Lin, K. F.; Tian, G.; Feng, Y.; Meng, X.; Di, Y.; Du, Y.; Zhang, Y.; Xiao, F. *Chem. Commun.* **2004**, 2612.
(54) Yang, X.; Zhang, S.; Qiu, Z.; Tian, G.; Feng, Y.; Xiao, F. S. *J. Phys. Chem. B* **2004**, *108*, 4696.

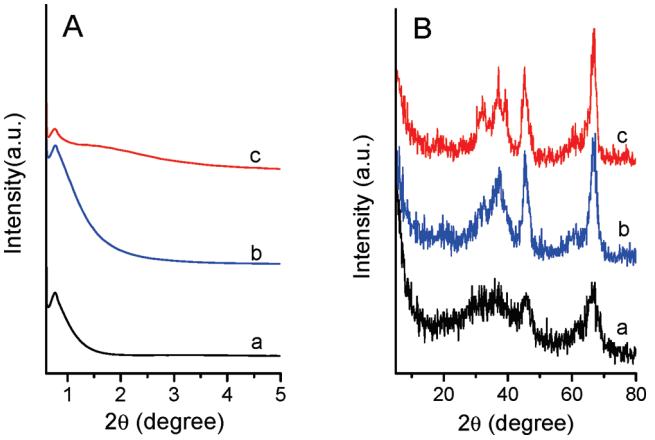

Figure 6. (A) Low-angle XRD patterns and (B) the corresponding wide-angle XRD patterns of the samples calcined at different temperatures and durations. (Legend: pattern a, 500 °C for 2 h; pattern b, 900 °C for 2 h; and pattern c, 900 °C for 48 h.)

Figure 6B), the boehmite AlOOH structure transformed to the γ-Al_2O_3 cubic phase (JCPDS File Card No. 29-0063). The result is consistent with previous reports that the γ-Al_2O_3 phase is formed upon dehydration of aluminum oxyhydroxide boehmite at temperatures in the range of 400−700 °C.[55] The diffractogram of the products calcined at 900 °C exhibits a relatively high degree of crystallinity, corresponding to γ-Al_2O_3.

FESEM and TEM observations of the thermally treated samples (Figures 7 and 8, respectively) directly confirm that no changes have occurred to either the monolithic porous foamlike morphologies with macroporous openings on the external surface (Figure 7), the macrocavity type texture, or the nanorod building blocks (Figure 8), indicating the high thermal stability of the 3D macroporous foamlike structure constructed from mesoporous nanorods. Notably, the crystalline phase of the product is maintained during thermal treatment, which can be observed in the SAED data, which have been inserted in the corresponding TEM images (Figure 8). Moreover, the electron diffraction patterns reveal that, after thermal treatment, intense diffraction spots progressively appeared on the diffraction rings, which indicates that the crystallinity of the γ-Al_2O_3 particles is gradually enhanced with increasing thermal treatment temperature and time. HRTEM observations of the nanofiber-like materials reveal direct evidence of sample crystallinity after thermal treatment (Figure 8d). After treatment at 900 °C for 2 days, nanofibers with a high degree of crystallinity are observed. The lattice fringes of 0.227 nm correspond to the (222) crystal plane of cubic γ-Al_2O_3 (see Figure 8d).

Furthermore, the ^{27}Al MAS NMR spectrum of the as-synthesized product (Figure 9) provides direct evidence of the extent of alumina condensation. The ^{27}Al MAS NMR spectra of the as-synthesized product (Figure 9a) and the calcined products (Figures 9b, c, and d) at various temperatures and times show three asymmetric lines, having maxima at 65, 33, and 7 ppm. According to the literature,[19] these bands are assigned to the central $\langle -^1/_2, ^1/_2 \rangle$ transition

(55) Ren, T. Z.; Yuan, Z. Y.; Su, B. L. *Langmuir* **2004**, *20*, 1531.

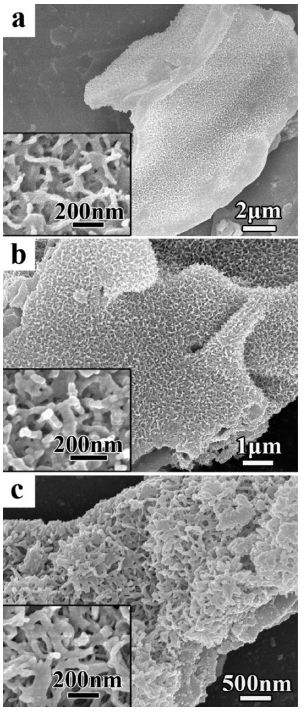

Figure 7. SEM images of the samples calcined at different temperatures and durations: (a) 500 °C for 2 h, (b) 900 °C for 2 h, and (c) 900 °C for 48 h. The insets are the corresponding higher-magnification views taken from the center of the same images.

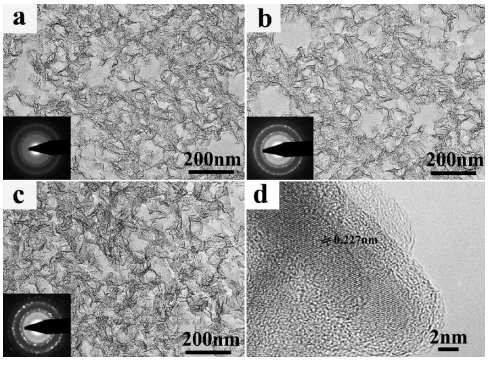

Figure 8. TEM images of the samples calcined at different temperatures and durations: (a) 500 °C for 2 h, (b) 900 °C for 2 h, and (c) 900 °C for 48 h. Panel (d) shows the HRTEM image of the nanofiber structure. The insets in the TEM images are the corresponding SAED patterns.

of the Al^{3+} ion in 4-fold (AlO_4), 5-fold (AlO_5), and 6-fold (AlO_6) coordination, respectively. The asymmetric line shape observed in the spectra reflects a distribution of isotropic chemical shifts, the asymmetry parameter, and the quadrupolar couplings, which was simulated using a simple model previously published.[56−58] One notices that the as-synthesized sample is mainly composed of hexacoordinated Al^{3+} ions, corresponding to the AlOOH boehmite intermediate phase, which is in good agreement with the XRD result (Figure 3b). After thermal treatments up to 500 °C for 2 h, Al^{3+} ions are distributed between the three

(56) Stebbins, J. F. In *Handbook of Physical Constants*, Vol. *2*; Ahrens, T. J., Ed.; American Geophysical Union: Washington, DC, 1995.
(57) Vaudry, F.; Khodabandeh, S.; Davis, M. E. *Chem. Mater.* **1996**, *8*, 1451.
(58) Yang, X.; Vantomme, A.; Lemaire, A.; Xiao, F. S.; Su, B. L. *Adv. Mater.* **2006**, *18*, 2117.

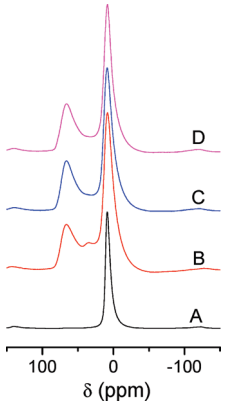

Figure 9. ^{27}Al magic angle spinning nuclear magnetic resonance (MAS NMR) spectra of the as-synthesized AlOOH product and the samples calcined at different temperatures and durations: as-synthesized AlOOH product (spectrum A), 500 °C for 2 h (spectrum B), 900 °C for 2 h (spectrum C), and 900 °C for 48 h (spectrum D).

sites of coordination with a clear tendency toward AlO_5, which is attributed to defects created by the large surface area of the network. Crystallization is complete after a treatment at 900 °C for 2 h, which is accompanied by the disappearance of the AlO_5 population, because of an increase in AlO_6 sites. Only AlO_6 and AlO_4 sites are subsequently observed, which is characteristic of the γ-Al_2O_3 phase. The maximal values expected, which are ~40% (AlO_4) and ~60% (AlO_6), typical to the γ- Al_2O_3 phase, is also verified. The products treated at 900 °C for 48 h gave a similar NMR spectrum. Very pure, well-crystallized, and thermally stable γ-Al_2O_3 materials with a well-organized 3D hierarchically macroporous foam structure with mesoporous nanorods as the building framework have been successfully synthesized.

3.2. Mechanistic Consideration: An In Situ Optical Microscopy Study. A high-resolution in situ optical microscope (80× magnification) was specially adapted to follow and directly observe the entire synthesis procedure. Each step of the synthesis, from the introduction of the precursor into the aqueous solution to the formation of the final gelatinous materials, was recorded. Based on this comprehensive optical microscopy study and the intensive characterization of the products obtained at different stages by FESEM, (HR)TEM, XRD, N_2 adsorption, and mercury porosimetry, and because of the chemistry of alkyl metals in aqueous solution, a formation mechanism is proposed. It is suggested that the alkyl aluminum molecule plays the role of a 2-in-1 precursor; i.e., it has two functions (precursor to the final product and generation of a molecular porogene) in one sole molecule, similar to the metal alkoxides used previously.[13−15,20,21,40−44,46−48,55,58,59] In contrast to metal alkoxides, the porogene molecules generated in the present case are gaseous methane molecules. When a droplet of TMA is added into an aqueous solution, a gelatinous thin layer is immediately formed at the surface of the water. This layer is composed of fibrous nanoparticles.[55] The droplet shape disappears and the

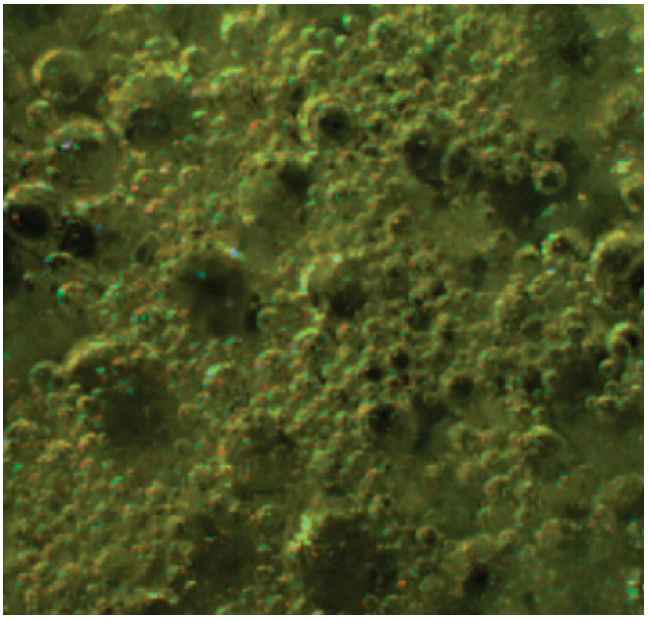

Figure 10. Optical microscopy (OM) image taken during the synthesis process.

gaseous methane that forms instantaneously evaporates out of the film; then, macro-apertures at the external surface of the film are formed. Direct observation by in situ optical microscopy witnesses the violent expulsion of gaseous methane. Figure 10 depicts one optical microscope image taken during the initial step of the synthesis procedure. We can see the very fast generation of a large number of bubbles. The photograph shown in Figure 1a reveals that the film was swollen because of the generation of gaseous methane. As illustrated in Scheme 1, the hydrolysis and condensation of TMA generate a large number of small nanoparticles with the release of methane molecules (step A in Scheme 1). These nanoparticles assemble together, forming a single nanofiber (step B in Scheme 1). This is well-evidenced by HRTEM (Figure 3c). As the reaction progresses, aggregation of the nanofibers occurs, leading to the formation of mesoporous nanorods (step C in Scheme 1). The mesoporosity is generated by this nanofiber scaffold, as previously reported.[18] The mesoporous nanorods used to construct macrocavities are clearly observed (Figure 3b). Then, branched mesoporous rods are formed (step D in Scheme 1). All these straight and branched nanorods assemble together to form the cagelike macrocavities around the methane bubbles (steps E and F in Scheme 1). Thus, a reasonably porous, 3D cage with macrocavities interconnected by mesoporous rods is produced. Note that the macrocavities are quite uniform, with homogeneously sized openings. This is most likely due to the very homogeneous phase separation procedure. Probably, the spontaneous CH_4 foam could bear a low water volume fraction; thereby, the pressure within the bubbles is homogeneous, providing homogeneous macroscopic void spaces to the entire sample, despite the fast reaction rate. Finally, the release of methane molecules from the hydrolysis reaction is quite homogeneous, thus leading to not only very

(59) Leonard, A.; Vantomme, A.; Bouvy, C.; Moniotte, N.; Mariaulle, P.; Su, B. L. *Nanopages* **2006**, *1*, 1.

Scheme I. Schematic Representation of the Proposed Synthesis Mechanism[a]

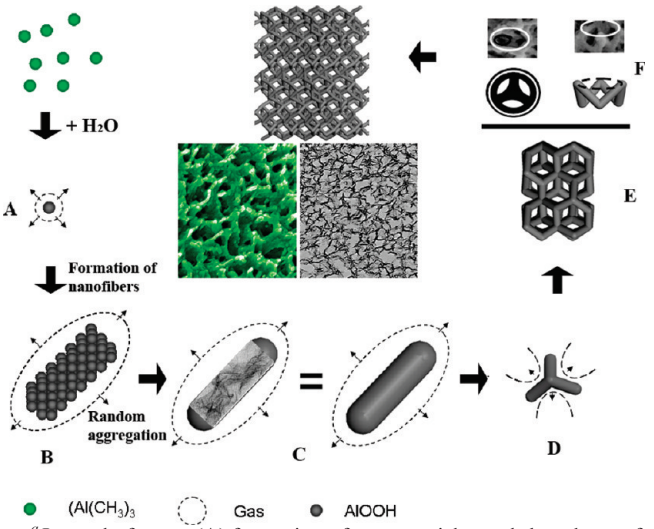

[a] Legend of steps: (A) formation of nanoparticles and the release of methane molecules; (B) aggregation of nanoparticles, leading to the formation of nanofibers; (C) random assembly of nanofibers, giving the formation of mesoporous rods with a wormlike mesostructure; (D) formation of branched rods; (E) formation of cagelike macrocavities around methane bubbles that act as the porogene; and (F) formation of 3D crystalline macroporous framework with mesoporous rods as walls.

homogeneous mesoporous nanorods but also the subsequent assembly of these mesoporous nanorods to form macrocavities within the cage. This type of structure allows a rapid discharge of large quantities of methane molecules instantaneously released during the hydrolysis of TMA. It is necessary to note that the hydrolysis and (poly)condensation reactions are so fast that steps B, C, D, and E can practically occur simultaneously. The reason why very porous openings are formed at the external surface of monolithic particles is because the gaseous methane molecules are expelled in the only possible direction, i.e., toward the exterior of the TMA layer. It is evident that the macroporous foamlike structures, interconnecting directly with and constructed from mesoporous nanorods, are spontaneously generated because of the power of the chemistry of alkyl aluminum.

The macroporosity derived from alkyl metal precursors is ~50−80 nm with homogeneous cagelike macrocavities, whereas metal alkoxides form funnel-like macrochannels with a diameter gradient from tens of nanometers up to several micrometers. The release of the gaseous methane, instead of alcohol molecules, leads to the clear difference in macrostructure of products obtained from two different 2-in-1 precursors. Moreover, the alcohol is hydrophilic, whereas methane is hydrophobic, which might favor the coalescence of inorganic species, resulting in two different pore diameters, particularly the big ones close to the surface. Very different hierarchically porous materials can be obtained just by changing the chemical precursor.

These novel crystalline 3D macroporous Al_2O_3 foams could radically improve existing Al_2O_3 applications, especially considering the ease at which production could be scaled up, because of not only the potential extension of this very simple synthesis method, but also the specific and very interesting 3D foamlike macrostructures with a homogeneous cagelike macroporous system interconnected with mesoporous walls.

4. Conclusions

We have fabricated a macroporous alumina with a hierarchical pore structure through a spontaneous procedure under mild conditions. In this synthesis process, trimethylaluminum ($Al(CH_3)_3$, TMA) was used and was the precursor of both the final product and the porogene (and, thus, was a so-called "two functions in one" (2-in-1) molecular precursor). The porogene bubbles (methane) released by hydrolysis of TMA played the most important role in producing the well-defined co-continuous macropores and wormlike mesopores. The phase transformation of boehmite crystallites to γ-Al_2O_3 was facilitated by a thermal process. Furthermore, the present work highlights the stabilization of a three-dimensional (3D) mesoporous−macroporous structure constructed from nanocrystalline frameworks at very high temperatures over a long time frame. By carefully selecting the chemical precursors, and on the basis of fast hydrolysis and condensation rates and the controlled release of self-generated, gaseous or liquid porogene molecules, unique and unprecedented porous hierarchies can be targeted. The improvement in performance in catalytic processes has been evidenced by this type of material.[60−69] This work also opens novel perspectives toward the elaboration of other types of interesting 3D mesoporous−macroporous crystalline materials, such as intrinsic semiconducting TiO_2 or SnO_2.

Acknowledgment. This work was realized in the frame of an Interuniversity Attraction Poles Program (Inanomat-P6/17)-Belgian State-Belgian Science Policy and the project "Redugaz", financially supported by the European community and the Wallon government in the frame of Interreg IV (France-Wallonie). X.Y.Y. thanks FNRS (Fonds National de la Recherche Scientifique, Belgium) for a position of "Chargé de Recherche". B.L.S. acknowledges the Chinese Central Government for an "Expert of the State" position in the Program of "Thousand Talents" and the Chinese Ministry of Education for a Changjiang Scholar position at the Wuhan University of Technology.

(60) Santacruz, I.; Nieto, M. I.; Moreno, R.; Faraldos, M.; Sastre, E. *Adv. Mater.* **2005**, *7*, 858.
(61) Bosc, F.; Lacroix-Dasmazes, P.; Ayal, A. *J. Colloid Interface Sci.* **2006**, *304*, 545.
(62) Pega, S.; Boissière, C.; Grosso, D.; Azais, T.; Chaumonot, A.; Sanchez, C. *Angew. Chem., Int. Ed.* **2009**, *48*, 2784.
(63) Idakiev, V.; Tabakova, T.; Yuan, Z. Y.; Su, B. L. *Appl. Catal., A* **2004**, *270*, 135.
(64) Idakiev, V.; Tabakova, T.; Naydenov, A.; Yuan, Z. Y.; Su, B. L. *Appl. Catal., B* **2006**, *63*, 178.
(65) Tidahy, H. L.; Siffert, S.; Lamonier, J. F.; Zhilinskaya, E.; Aboukais, A.; Yuan, Z. Y.; Vantomme, A.; Su, B. L.; Canet, X.; De Weireld, G.; Frere, M.; N'Guyen, T.; Giraudon, J.; Leclercq, G. *Appl. Catal., A* **2006**, *310*, 61.
(66) Hosseini, M.; Siffert, S.; Tidahy, H. L.; Cousin, R.; Lamonier, J.; Aboukais, A.; Vantomme, A.; Roussel, M.; Su, B. L. *Catal. Today* **2007**, *122*, 391.
(67) Yuan, Z. Y.; Idakiev, V.; Vantomme, A.; Tabakova, T.; Ren, T. Z.; Su, B. L. *Catal. Today* **2008**, *131*, 203.
(68) Tidahy, H. L.; Hosseni, M.; Siffert, S.; Cousin, R.; Lamonier, J. F.; Aboukais, A.; Su, B. L.; Giraudon, J. M.; Leclercq, G. *Catal. Today* **2008**, *137*, 335.
(69) Giraudon, J. M.; Nguyen, T. B.; Leclercq, G.; Siffert, S.; Lamonier, J. F.; Aboukais, F. A.; Vantomme, A.; Su, B. L. *Catal. Today* **2008**, *137*, 379.